Loss of *cerebral cavernous malformation 3* (*Ccm3*) in neuroglia leads to CCM and vascular pathology

Angeliki Louvi[a,1], Leiling Chen[a], Aimee M. Two[a], Haifeng Zhang[b,c], Wang Min[b,c], and Murat Günel[a,c,d,1]

[a]Departments of Neurosurgery and Neurobiology, Yale Program on Neurogenetics, [b]Department of Pathology, [c]Interdepartmental Program in Vascular Biology and Therapeutics, and [d]Department of Genetics, Yale School of Medicine, New Haven, CT 06520

Edited by Christine E. Seidman, Harvard Medical School, Boston, MA, and approved January 12, 2011 (received for review August 25, 2010)

Communication between neural cells and the vasculature is integral to the proper development and later function of the central nervous system. A mechanistic understanding of the interactions between components of the neurovascular unit has implications for various disorders, including cerebral cavernous malformations (CCMs) in which focal vascular lesions form throughout the central nervous system. Loss of function mutations in three genes with proven endothelial cell autonomous roles, *CCM1/krev1 interaction trapped gene 1*, *CCM2*, and *CCM3/programmed cell death 10*, cause familial CCM. By using neural specific conditional mouse mutants, we show that *Ccm3* has both neural cell autonomous and nonautonomous functions. *Gfap*- or *Emx1*-Cre–mediated *Ccm3* neural deletion leads to increased proliferation, increased survival, and activation of astrocytes through cell autonomous mechanisms involving activated Akt signaling. In addition, loss of neural CCM3 results in a vascular phenotype characterized by diffusely dilated and simplified cerebral vasculature along with formation of multiple vascular lesions that closely resemble human cavernomas through cell nonautonomous mechanisms. RNA sequencing of the vascular lesions shows abundant expression of molecules involved in cytoskeletal remodeling, including protein kinase A and Rho-GTPase signaling. Our findings implicate neural cells in the pathogenesis of CCMs, showing the importance of this pathway in neural/vascular interactions within the neurovascular unit.

cerebrovascular disease | activated astrocytes | animal models

Cerebral cavernous malformations (CCM) affect ~0.5% of the general population and are characterized by dilated sinusoidal vascular spaces lined by a single layer of endothelium, lacking all other normal vessel-wall elements and central nervous system (CNS) tissue (1). CCM affects both brain and spinal cord and rarely, retina and skin. Only about one-third of affected individuals develop clinical symptoms, which include intracranial hemorrhage and seizures (2). CCM can be sporadic or familial, and more than 90% of patients with autosomal dominant CCM carry loss of function mutations in one of three genes: *CCM1*/*krev1 interaction trapped gene 1* (*KRIT1*), *CCM2*, and *CCM3*/*programmed cell death 10* (*PDCD10*) (3). CCM is thought to result from a two-hit mechanism (4), and in a limited number of samples, biallelic somatic mutations in one of the *CCM* genes have been identified in endothelial cells lining cavernous vessels of patients with germline mutations (5, 6), supporting the notion that the primary defects in CCM can be specific to the endothelium. However, in addition to the arterial endothelial cells, the *CCM* genes are expressed in cortical pyramidal neurons and astrocytes (7–9). These observations and the fact that CCM lesions are almost exclusively confined to the CNS lead to the hypothesis that vascular lesions may arise because of abnormalities in surrounding cells, such as neuroglia, rather than defects intrinsic to the endothelium (10), an idea that has yet to be formally proven.

In mice, *Ccm1* deletion results in embryonic lethality associated with defects in arterial morphogenesis (11). Although $Ccm1^{+/-}$ mice seem normal, in the absence of p53 function or in a sensitized background deficient for mismatch repair, approximately one-half develop lesions resembling CCM (12, 13). Similarly, *Ccm2* deletion causes embryonic lethality, and ~10% of *Ccm2* heterozygotes develop lesions (10). *Ccm2* inactivation in the endothelium causes cardiovascular pathology; however, both neural and vascular smooth muscle conditional mutants seem normal (14–16). CCM2 acts cell autonomously in the endothelium, affecting cell junctions and consequently, vessel integrity (14, 16). In addition, CCM2 signaling has been shown to be important in mediating cell death induced by the neurotrophic tyrosine kinase receptor type 1 (TrkA) receptor tyrosine kinase (17).

The molecular function of CCM3 remains under intense study. Biochemical and structural studies have indicated that CCM3 can participate in a protein complex also containing CCM1 and CCM2 (18, 19), which directly interact with each other (20, 21), and that CCM3 binds CCM2 through its C-terminal domain (22). CCM3, however, has also been identified as part of an additional multiprotein complex that includes all three members of the germinal center kinase III (GCK-III) family of Ste20 kinases [serine/threonine kinase (Stk) 24, Stk25, and Mst4] (23), possibly promoting assembly of the Golgi apparatus (24). Interestingly, many components of this complex are involved in cell cycle regulation and apoptosis, with CCM3 having a proapoptotic role in vitro (25). Finally, global or endothelial deletion of *Ccm3* causes embryonic lethality associated with defects in vascular development and VEGF receptor 2 (VEGFR2) signaling (26), and in zebrafish, CCM3-mediated signaling through Ste20-like kinases is involved in cardiovascular development (27).

Here, we examine the role of *Ccm3* in neurovascular development and disease. We show that loss of *Ccm3* in neural cells has cell autonomous effects causing activation of astrocytes through Akt signaling in addition to cell nonautonomous effects in the vasculature, including a diffusely dilated and simplified vascular tree and formation of lesions that resemble typical human cavernomas.

Results

Generation of *Ccm3* Neural Mutants. To explore the function of CCM3, we generated tissue-specific *Ccm3* knockouts. The generation of the $Ccm3^{lox}$ allele (*SI Materials and Methods*) and mutants with global and endothelial deletion of *Ccm3* has been reported (26). To study its neural-specific functions, we ablated *Ccm3* using three Cre lines that direct recombination in partially overlapping populations of neural cells with temporally and

Author contributions: A.L. and M.G. designed research; A.L., L.C., and A.M.T. performed research; H.Z. and W.M. contributed new reagents; A.L., L.C., A.M.T., and M.G. analyzed data; and A.L. and M.G. wrote the paper.

The authors declare no conflict of interest.

This article is a PNAS Direct Submission.

Data deposition: The data reported in this paper have been deposited to the NCBI short read archive, http://trace.ncbi.nlm.nih.gov/Traces/sra/sra.cgi.

[1]To whom correspondence may be addressed. E-mail: angeliki.louvi@yale.edu or murat.gunel@yale.edu.

This article contains supporting information online at www.pnas.org/lookup/suppl/doi:10.1073/pnas.1012617108/-/DCSupplemental.

spatially different profiles: *Nestin*-Cre (28), *Gfap*-Cre (29), and *empty spiracles homolog 1* (*Emx1*)-Cre (30) (*SI Materials and Methods*). Importantly, none of these Cre lines are active in endothelial cells (30, 31). In mutant animals, expression of *Ccm3* mRNA and protein was significantly down-regulated compared with controls (Fig. S1).

Neural Cell Autonomous Functions of CCM3. To examine CCM3 function in neural cells, we initially deleted *Ccm3* by generating *Nestin*-Cre;$Ccm3^{lox/lox}$ (*Nestin-Ccm3*) mutants (*SI Materials and Methods*). Mutant animals were born in lower than expected Mendelian ratios and did not survive past postnatal day 3 (P3); their main feature was an enlarged brain with abnormal cytoarchitecture, suggesting that *Ccm3*, in addition to its role in endothelial cells (26), has a cell autonomous neural function. To further study the neural phenotype in viable *Ccm3* neural mutants, we tested the *Gfap*- and *Emx1*-Cre drivers (*SI Materials and Methods*).

The *Gfap*-Cre;$Ccm3^{lox/lox}$ (*Gfap-Ccm3*) mutants were born in expected Mendelian ratios but similar to the *Nestin-Ccm3* animals, also suffered a high mortality rate (~80%) at around 4 wk. The *Gfap*-Cre mutants failed to thrive and had reduced body weight; their brains, however, were large (Fig. S2), with dilated ventricles and abnormal cytoarchitecture. The remaining one-fifth of *Gfap-Ccm3* animals that did survive to adulthood weighed ~65% of control littermates at weaning and had a shorter lifespan (none survived beyond 12 mo). These also had enlarged brains (Fig. S2). All *Gfap-Ccm3* animals had significant neurological findings, including unsteady gait and circling.

Unlike the *Nestin*- and *Gfap-Ccm3* mice, all *Emx1*-Cre; $Ccm3^{lox/lox}$ (*Emx1-Ccm3*) mutants, born in expected Mendelian ratios, survived to adulthood. Although they seemed grossly healthy, the overall phenotypic findings, including large brains, were similar to the other two mutants (Figs. S1 and S3).

The increased brain size in the three *Ccm3* neural mutants suggested neural cell autonomous effects of CCM3. In *Gfap*- and *Emx1-Ccm3* mutants, a progressive increase in reactive astrocytes highly expressing the intermediate filaments *Gfap* and *vimentin* was observed starting at early postnatal stages (Fig. 1 and Fig. S3). We, therefore, isolated primary cortical astrocytes in which *Ccm3* is deleted from *Gfap-Ccm3* and control littermates at P3 (Fig. 2*A*), and we tested basic cellular functions such as proliferation and apoptosis. Consistent with our previous observations (25), *Ccm3* mutant astrocytes showed both increased proliferation (Fig. 2 *B* and *C*) and resistance to cycloheximide-induced apoptosis (Fig. 2*D*) and had reduced levels of activated caspase-3 compared with controls (Fig. 2*E*). Furthermore, in mutant astrocytes, the early apoptotic fraction was significantly decreased, suggesting increased survival (Fig. 2*F*).

Given the prosurvival phenotype of mutant astrocytes, we next examined Akt signaling, which has documented effects on proliferation and cell survival/apoptosis suppression (32). Baseline levels of activated (phospholylated) Akt were increased in *Ccm3* mutant astrocytes and remained elevated even after serum withdrawal, a treatment that decreased phosphorylated Akt (pAkt) in control astrocytes. Consistent with this, the levels of phosphorylated forkhead box O1 (FoxO1), a downstream target of Akt, were also increased (Fig. 2*G*).

Vascular Pathology in *Ccm3* Neural Mutants. Given the abundance of reactive astrocytes in *Ccm3* neural mutants and the fact that astrocytes are important for neural/vascular interactions within the neurovascular unit (33), we examined the cerebrovasculature. Capillaries in *Gfap-Ccm3* brains seemed less organized than in controls (Fig. 3 *A* and *E*). Moreover, cerebral vessels (visualized by intravascular administration of a biotinylated tracer to label endothelial surface proteins) were dilated in *Gfap-Ccm3* mutants at all ages examined ($n = 7$; P20 to 10 mo) (Fig. 3 *B* and *F*). The tracer remained confined within the vasculature,

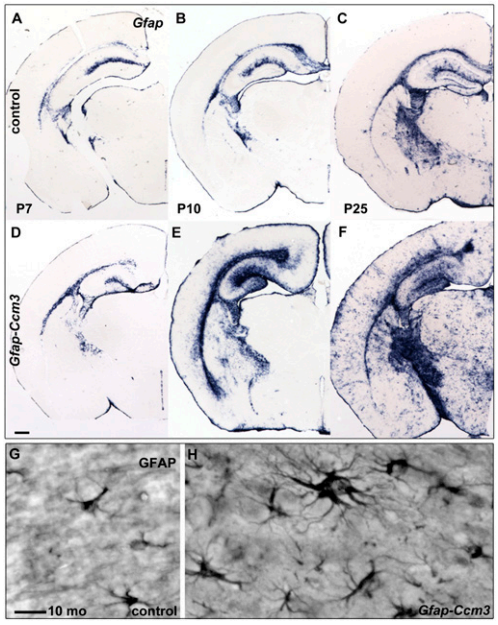

Fig. 1. Progressive accumulation of activated astrocytes in *Gfap-Ccm3* animals. (*A–F*) *Gfap* mRNA detected with in situ hybridization is progressively increased in *Gfap-Ccm3* mutants (*D–F*) compared with control littermates (*A–C*). Results are representative of multiple (>50) paired observations at P7, P10, P25, and additional developmental stages. (*G* and *H*) Morphology of cortical astrocytes in control (*G*) and *Gfap-Ccm3* (*H*) animals (10 mo) revealed with immunohistochemistry with GFAP. Results are representative of multiple (>10) paired observations at various developmental stages. (Scale bars: *A–F*, 0.5 mm; *G* and *H*, 20 μm.)

suggesting that neural deletion of *Ccm3* had no generalized effects on the integrity of the blood–brain barrier, and ultrastructural analyses revealed normal endothelial tight junctions in the dilated vessels examined (Fig. S4 *A–D*). In addition, vessel density was decreased significantly in the *Gfap-Ccm3* mutants at all ages examined ($n = 5$; P21 to 10 mo) (Fig. 3 *B*, *C*, *F*, and *G* and Fig. S4*E*). *Connexin43* mRNA, encoding a gap junction protein that connects astrocytic end-foot processes, was lower in perivascular astrocytes around large- and medium-sized vessels (Fig. 3 *D* and *H*). These observations suggest that *Ccm3* neural deletion has cell nonautonomous effects in the cerebrovasculature.

To further confirm the cell nonautonomous effects of *Ccm3* neural deletion, we examined the retinal vasculature, which develops postnatally on a template of astrocytes migrating from the optic nerve (34). Retinal astrocytes derive from *Gfap*-expressing progenitors (Fig. 3*I*) and therefore, are deficient for CCM3 in the *Gfap-Ccm3* mutants. In control P2 pups, astrocytes emerging from the optic nerve head have spread across the inner surface of the retina (Fig. 3*J*), forming a network for the endothelial cells to follow (Fig. 3*M*). In *Gfap-Ccm3* littermates, spreading of astrocytes was attenuated (Fig. 3 *K* and *L*); as a consequence, endothelial cell migration was delayed (Fig. 3 *N* and *O*).

Because of their interactions with blood vessels initiated during postnatal gliogenesis (35) and their role in the control of local microcirculation, astrocytes have been proposed to be involved in cerebrovascular regulation (36). Our observations of dilated vessels in an environment of abundant activated astrocytes prompted us to examine molecules expressed at the astrocyte/vessel interface. One candidate is Angiopoietin 1 (Ang1), which is expressed by astrocytes surrounding blood vessels (37), acts through Akt pathway activation (38), and when overexpressed in forebrain neurons or delivered systemically, causes

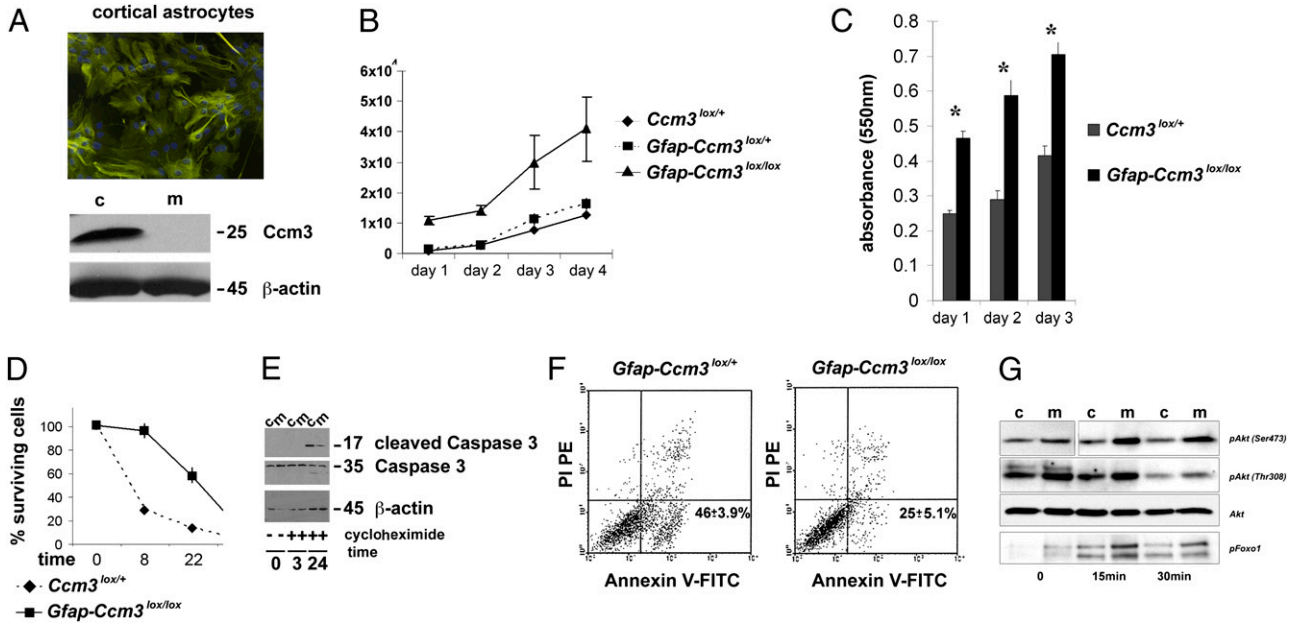

Fig. 2. Increased proliferation and survival in *Ccm3* mutant astrocytes. (*A*) Immunofluorescent staining for intermediate filaments (GFAP) and nuclei (DAPI) in primary astrocytes isolated from P3 neocortex (*Upper*). Immunoblot analyses of cell lysates for CCM3 prepared from astrocytic cultures established from *Ccm3*$^{lox/+}$ (control) and *Gfap-Ccm3* (mutant) littermates (*Lower*). Results are representative of multiple (>15) independent experiments. (*B*) Proliferation curve of control and *Ccm3* mutant astrocytes. Results are representative of three independent experiments. (*C*) Cell proliferation determined by absorbance at 550 nm using the 3-(4,5-dimethylthiazol-2-yl)-2,5-diphenyl tetrazolium (MTT; 0.5 mg/mL) assay. (*D*) Cell survival assay after treatment with cycloheximide (20 μg/mL). Cells were harvested and counted at indicated time points. Results are representative of three independent experiments. (*E*) Immunoblot analyses of cell lysates for cleaved (active) caspase 3 and total caspase 3 after treatment with cycloheximide (20 μg/mL). Results are representative of three independent experiments. (*F*) Flow cytometric analysis of *Gfap-Ccm3*$^{lox/+}$ control (*Left*) and *Ccm3* mutant (*Right*) astrocytes 24 h after treatment with cycloheximide. The lower left quadrant in *Left* and *Right* shows viable cells (annexin V−/PI−). The lower right quadrant in *Left* and *Right* shows early apoptotic cells (annexin V+/PI−). The upper right quadrant in *Left* and *Right* shows late apoptotic/necrotic cells (annexin V+/PI+). The upper left quadrant in *Left* and *Right* shows necrotic cells (annexin V−/PI+). Results similar to those from *Gfap-Ccm3*$^{lox/+}$ control astrocytes were obtained with *Ccm3*$^{lox/+}$ and *Ccm3*$^{lox/lox}$ astrocytes. (*G*) Immunoblot analyses of cell lysates prepared from astrocytic cultures established from *Ccm3*$^{lox/+}$ (c, control) and *Gfap-Ccm3* (m, mutant) littermates. Immunoblot analyses for pAkt (Ser473), pAkt (Thr308), Akt, and pFoxO1 at steady state and after serum withdrawal for times indicated. Results in *B–F* are representative of five paired independent experiments. Values in *B–F* are means ± SD. Results in *G* are representative of two independent experiments.

vessel enlargement (37, 39). In control brains, as expected (37), Ang1 accumulated around blood vessels and neurons (Fig. 3 *P*, *R*, and *T*), which was also the case in mutant brains (Fig. 3 *Q* and *S*). However, activated astrocytes in both *Gfap-* and *Emx1-Ccm3* mutants showed a dramatic increase in Ang1 expression throughout the brain (Fig. 3 *U* and *V*).

Formation of Vascular Lesions in *Ccm3* Neural Mutants. Given their vascular phenotype and the known role of CCM3 in lesion formation, we next examined adult *Gfap-* and *Emx1-Ccm3* brains for evidence of pathology. To our surprise, two-thirds (21 of 31) of *Gfap-Ccm3* mice (3 wk to 12 mo) had developed one (8 of 21) or even a few (13 of 21) cerebrovascular lesions that resembled human CCMs with the characteristic raspberry-like appearance of cavernomas (Figs. 4 and 5, Fig. S5, and Table S1). The lesions were usually superficial (18 of 21) and formed throughout the brain as well as in the spinal cord. Interestingly, young animals (3–8 wk of age; $n = 6$) that developed lesions also had severe hydrocephalus (Fig. 4*G* and Table S1). Onset of lesion formation was not systematically examined. Remarkably, lesions were never observed in *Gfap-Ccm3* mutants analyzed between birth and weaning (P21; $n > 100$). Similarly, over 80% (10 of 12) of the *Emx1-Ccm3* animals (7 mo and older) developed one ($n = 1$) or multiple ($n = 9$) lesions (Table S1), also predominantly superficial (8 of 10) and confined to the forebrain, reflecting the restricted expression of *Emx1*-Cre (Figs. 4*H* and 6*C*, Fig. S5 *A* and *I*, and Table S1). Two *Gfap-Ccm3* and two *Emx1-Ccm3* animals had deep lesions within the parenchyma (Fig. 6 *A–C*, Figs. S5*H* and S6 *G–I*, and Table S1).

Analyses of CCM-Like Vascular Lesions. The lesions developing in *Gfap-* and *Emx1-Ccm3* mice consisted of thin-walled dilated clustered microvessels lined with a single layer of endothelium without intervening parenchyma, similar to human cavernomas (Fig. 5 *A–E* and Fig. S6 *S–U*). Ultrastructural analyses revealed both luminal and abluminal erythrocytes (Fig. 5*F*), indicating extravasation and microhemorrhage within the lesion; however, there was no hemorrhage in the vasculature outside the lesion, and hemosiderosis was limited, in contrast to human lesions (Fig. S6 *S–U*). Some properly formed endothelial tight junctions were evident (Fig. 5*G* and Fig. S7), and numerous platelets were present within the lumen (Fig. 5*H*), consistent with observations of frequent thrombi in human CCM (40).

The lesions were surrounded by foci of high cellular proliferation (Fig. 6*A*) and abundant activated astrocytes expressing high levels of *Gfap* (Fig. 6 *B* and *C*) compared with lesion-free areas of the same mutant brain, suggesting a possible link between lesion formation and astrogliosis. Consistent with our in vitro observations, significant pAkt and Ang1 expression was detected in areas immediately surrounding the lesions (Fig. 6 *D–G*). Remarkably, in these areas, one of the downstream targets of Akt signaling that mediates its vascular effects, nitric oxide synthase (NOS), was also up-regulated (Fig. 5*D* and Fig. S6*B*).

RNA Sequencing of CCM-Like Vascular Lesions. To gain mechanistic insights into the CCM-like lesions, we used RNA sequencing (RNA-seq) to examine their transcriptional profile. Three lesions (i.e., three biological replicates) were microdissected from the cortical surface of three *Emx1-Ccm3* animals (7 mo). One had

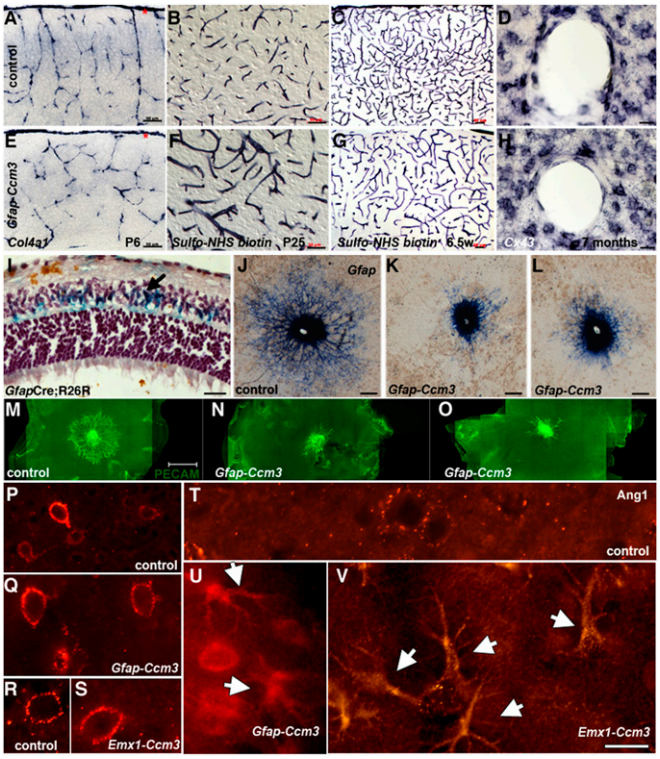

Fig. 3. Vascular phenotypes in *Ccm3* neural mutants. (*A* and *E*) Cortical vessels visualized by in situ hybridization for *collagen 4a1*. Vessels originating from the pial surface (red asterisks) and invading the cortex seem disorganized in *Gfap-Ccm3* mutants (*E*) compared with controls (*A*). Results are representative of three paired observations. (*B*, *C*, *F*, and *G*) Cerebral vasculature visualized after intracardiac administration of *N*-hydroxysulfosuccinimide (sulfo-NHS)-biotin. In *Gfap-Ccm3* mutants (*F* and *G*), the vessels are dilated (*F*), and the vascular tree is overall less complex (*G*) compared with controls (*B* and *C*). Results are representative of seven paired observations. (*D* and *H*) In situ hybridization staining for *connexin 43* (*Cx43*) indicates lower levels of *Cx43* mRNA expression in perivascular astrocytes of *Gfap-Ccm3* mutants (*H*) compared with controls (*D*). Results are representative of four paired observations. (*I*) X-gal histochemistry of retina from a 3-wk-old *Gfap*-Cre animal carrying the R26R reporter (*GfapCre;*R26R) shows that retinal astrocytes (blue and arrow) derive from *Gfap*-expressing progenitors. (*J–L*) In situ hybridization for *Gfap* in P2 retinas from one control (*J*) and two *Gfap-Ccm3* (*K* and *L*) animals. In control retinas (*J*), astrocytes emerging from the optic nerve spread in a centrifugal fashion; in mutants (*K* and *L*), astrocyte spreading is attenuated. Results are representative of six paired observations. (*M–O*) Immunostaining for platelet endothelial cell adhesion molecule 1 (PECAM-1) in P1 retinas from one control (*M*) and two *Gfap-Ccm3* mutants (*N* and *O*) shows retinal endothelial cells following the astrocytic network in controls (*M*) but are stalled in *Gfap-Ccm3* retinas (*N* and *O*). Results are representative of four paired observations. (*P–V*) Immunostaining for Angiopoietin-1 (Ang1) shows expression around cortical vessels and neurons in 7.5-wk-old control (*P*) and *Gfap-Ccm3* (*Q*) littermates and in 12-mo-old control (*R*) and *Emx1-Ccm3* (*S*) littermates. Expression in cortical astrocytes is low to undetectable in 12-mo-old controls (*T*) but dramatically up-regulated in 5.5-mo-old *Gfap-Ccm3* (*U*) and 12-mo-old *Emx1-Ccm3* mutants (arrows indicate activated astrocytes of characteristic morphology). Results are representative of three paired observations per genotype at different ages. (Scale bars: *A–D*, *G*, and *H*, 50 μm; *E*, *F*, and *I*, 20 μm; *J–L*, 200 μm; *M–O*, 500 μm; *P–V*, 20 μm.)

a single lesion, whereas the remaining two had multiple lesions (Table S1).

After mapping the RNA-seq data, we used fragments per kilobase of transcript per million fragments mapped (FPKM) as a measure of relative abundance of each transcript. In accordance with the literature (41), we considered any gene with FPKM > 20 in all three biological replicates to be moderately to highly abundant within the lesion. Of the 1,003 genes with

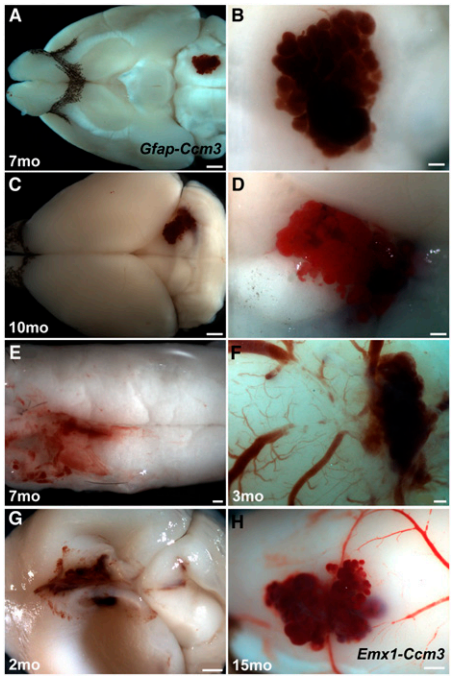

Fig. 4. Vascular lesions develop in *Ccm3* neural mutants. (*A–E*) Lesions resembling human cavernomas develop in the brains (*A–D*) and spinal cords (*E*) of *Gfap-Ccm3* animals. *B* and *D* are higher magnification views of *A* and *C*. (*F*) Lesion in a 3-mo-old *Gfap-Ccm3* animal that died accidentally. (*G*) Lesion in the dorsomedial cortex of a 2-mo-old animal with severe hydrocephalus, indicated by the collapsed cortical wall. (*H*) Cortical lesion in a 15-mo-old *Emx1-Ccm3* animal. Brains in *F* and *H* were extracted fresh without perfusion; cerebral surface vessels can be seen feeding into the lesion. (Scale bars: *A* and *C*, 1 mm; *B*, *D*, *E*, and *F*, 200 μm; *G* and *H*, 500 μm.)

FPKM > 20, 822 were common in all samples. We investigated these moderately to highly expressed genes using pathway analysis (http://www.genego.com/) to determine which signaling pathways are active in the lesions. Using enrichment analysis (EA) to identify dataset-specific *P* value distributions of transcripts in several functional ontologies, we identified cytoskeletal remodeling as the most significantly up-regulated pathway ($P < 2.2 \times 10^{-9}$ for each of the three samples analyzed) (Fig. S8) because of protein kinase A (PKA) expression (FPKM average ± SD is 43.82 ± 4.47) with activation of downstream Rho-GTPases, including the highly conserved mammalian Rho-GTPases, RhoA, Rac, and cell division cycle 42 homolog (CDC42), with RhoA being the most abundant (65.5 ± 7.0). Indeed, cytoskeletal proteins such as cytoskeletal β-actin (221.1 ± 49.5), fodrin (88.66 ± 10.72), and cofilin (101.6 ± 7.3) were highly abundant. These findings are consistent with previous studies, which suggested RhoA activation after *Ccm2* deletion (14) and CCM interactions with β1-integrins (42, 43) and offer a unique insight into lesion genesis and progression after neural *Ccm3* inactivation. Interestingly, *Ccm3* transcripts were detected in all three lesions analyzed by RNA-seq (2.7 ± 1.4), suggesting that CCM-like lesions in these neural mutants did not form because of lack of CCM3 in the endothelium.

Discussion

Here, we show that neural *Ccm3* deletion has cell autonomous effects in astrocytes, including increased cell proliferation and cell survival/resistance to apoptosis because of Akt pathway activation. Surprisingly, neural *Ccm3* deletion also results in a cell nonautonomous vascular phenotype characterized by diffuse dilation, decreased complexity of the vascular tree, and formation of lesions that closely resemble human CCM.

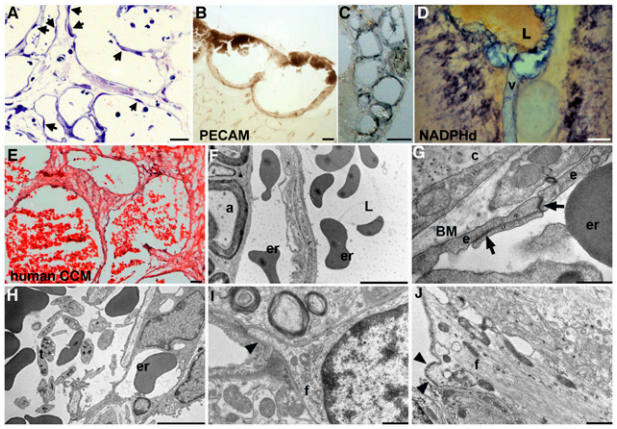

Fig. 5. Fine structure of lesions. (*A*) Toluidine blue staining of a semithin (0.7-μm) section of a lesion from a 7-mo-old *Gfap-Ccm3* animal. Endothelial cells line the dilated vascular channels (arrows indicate endothelial cell nuclei). (*B* and *C*) Immunohistochemical visualization of the endothelial lining (PECAM) of two lesions from 7- (*B*) and 10-mo-old (*C*) *Gfap-Ccm3* animals. (*D*) NADPH-diaphosase histochemical staining (NOS activity) of a lesion from a P24 *Gfap-Ccm3* animal with severe hydrocephalus. L, blood-containing lumen of dilated vessel (v) at the lesion site. Results are representative of multiple (>20) independent observations. (*E*) H&E staining of a human lesion resected from a patient with CCM. Multiple caverns lined with a single layer of endothelium are shown. (*F–J*) Representative transmission electron micrographs of lesions from two *Gfap-Ccm3* animals (*F*, 7-mo-old animal; *G–J*, 10-mo-old animal). Erythrocytes (er) are present both in the luminal (L) and abluminal sides of the dilated vessel. a, axon in neighboring parenchyma. (*G*) Tight junctions (arrows) between adjacent endothelial cells (e) lining the lesion. c, connective tissue; BM, basement membrane. (*H*) Intraluminal thrombocytes (t) within the lesion. (*I* and *J*) Cellular membrane (arrowheads) of astrocytic end-foot processes (f) abutting a dilated yet lesion-free vessel (*I*) or the vascular lesion proper (*J*) in the same brain. Note the electron-dense membrane of end foot abutting the lesion. (Scale bars: *A*, 20 μm; *B*, 200 μm; *C* and *D*, 50 μm; *E* and *G*, 5 μm; *F*, 500 nm; *H* and *I*, 1 μm.)

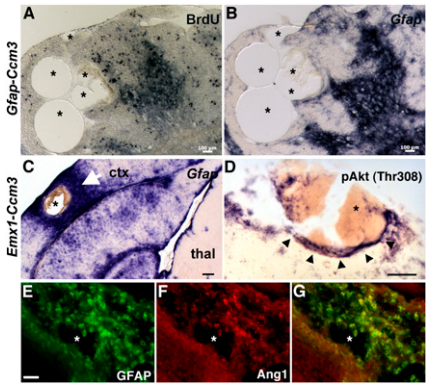

Fig. 6. Characterization of vascular lesions. (*A–C*) Multiple dilated vascular channels (asterisks) of a lesion from a 10-mo-old *Gfap-Ccm3* (*A* and *B*) and a 9-mo-old *Emx1-Ccm3* animal (*C*). (*A*) Foci of cellular proliferation close to the lesion but not within the endothelium after a single BrdU injection at embryonic day 15.5. (*B* and *C*) In situ hybridization staining for activated astrocytes (*Gfap*). In *C*, activated astrocytes are absent from thalamus (thal), where *Emx1*-Cre is not expressed; arrow indicates extensive astrogliosis immediately surrounding the lesion (asterisk) in lateral neocortex (ctx). (*D*) pAkt (Thr308) is up-regulated (arrowheads) in cells surrounding a lesion (asterisk indicates blood within the dilated vasculature) in a 5.5-wk-old *Gfap-Ccm3* mutant. (*E–G*) Immunostaining for GFAP (*E*) and Angiopoietin-1 (Ang1; *F*) of a lesion from a 7.5-wk-old *Gfap-Ccm3* animal. Asterisk indicates a dilated vascular channel within the lesion. *G* is a merged image of *E* and *F*. Results are representative of three independent observations. (Scale bars: *A* and *B*, 100 μm; *C*, 200 μm; *D–G*, 50 μm.)

Our findings provide in vivo evidence that a CCM gene, *Ccm3*, is required for normal physiologic function in nonvascular cells and implicate a cell nonautonomous mechanism in disease pathogenesis, suggesting that CCM lesions can develop as a result of altered interactions within the neurovascular unit. This finding has significant implications and potentially explains why CCM lesions develop almost exclusively in the CNS, including the retina, despite widespread expression of CCM proteins. Indeed, dysfunctional cell–cell signaling has been associated with other CNS pathologies, most notably inherited amyotrophic lateral sclerosis, in which astrocytes contribute to motor neuron loss through cell nonautonomous mechanisms (44). Likewise, cerebral hemorrhages have been reported in mice lacking α_v-integrins in astrocytes (45). Interestingly, germ cell death in *Caenorhabditis elegans* is regulated by *kri-1* expressed in somatic tissues through a cell nonautonomous mechanism (46).

Importantly, our analysis revealed that, in *Ccm3* mutants, cell autonomous neural and nonautonomous vascular abnormalities precede the onset of lesion formation. Despite widespread vascular pathology, the observed CCM lesions, similar to human disease, are focal and age-dependent. In that respect, our observation that young animals only develop lesions in conjunction with severe astrocytosis at the lesion site suggests that injury may play a role in lesion formation, a notion consistent with clinical reports of CCM developing or expanding after physical trauma, injury, or radiation (47, 48). Why lesions preferentially form on the surface of the brain in the *Ccm3* mutants is not understood.

The finding that neural loss of *Ccm3* but not *Ccm2* (14, 15) leads to neural and vascular phenotypes, including lesions, further implies that the molecular signature of CCM may be distinct depending on the gene mutated. Indeed, mutations in the *CCM* genes have varying degrees of clinical penetration; clinical manifestations may also vary, and individuals with *CCM3* mutations are at greater risk for more aggressive clinical course and highest rates of hemorrhage (49, 50). Finally, our findings indicate that the primary defects in CCM need not be endothelial-specific, contrary to what has been suggested by the absence of cerebrovascular defects in neural *Ccm2* mutants (14, 15) as well as the presence of somatic mutations in endothelial cells lining human lesions (5, 6).

Our study links CCM3 function to neural–vascular communication within the neurovascular unit. This is reminiscent of the Ang–Tie interactions coupling the mesenchymal compartment with the endothelium. Activating mutations in Tie2 result in peripheral venous malformations that resemble CCM lesions (51). In neural *Ccm3* mutants, there is increased Ang-1 expression, potentially activating Tie2 in endothelial cells. Indeed, at the light microscopy level, CCM closely resemble venous malformations, with nearly lack of any vascular wall elements except endothelial cells and disruption of cell–cell interactions underlying their pathophysiology.

In summary, our observations potentially explain why CCM lesions are predominantly CNS-specific, focal, and dynamic. Although clinically asymptomatic in most cases, CCM lesions can cause debilitating problems. The only accepted treatment modality is microsurgical resection, with its associated risks. The mouse model that we developed replicates many aspects of human CCM, allowing mechanistic insights, which include the cell autonomous and nonautonomous functions of CCM3, the involvement of Akt signaling, and cytoskeletal remodeling because of PKA and Rho-GTPase activation within the vascular lesions. Significantly, altered CCM signaling in neuroglia might have implications for other findings in CCM, including seizures. Further dissecting these pathological mechanisms will allow for a more detailed understanding of CCM biology, provide important insights into the role of cell–cell signaling within the neuro-

vascular unit, and potentially, pave the way for rational therapeutic approaches.

Materials and Methods

Mice were maintained in compliance with National Institutes of Health guidelines and approval of the Yale University Institutional Animal Care and Use Committee. *Ccm3* conditional mutant mice were generated as previously described (26). Detailed methods on mice, in situ hybridization, immunohistochemistry, other histochemical methods, EM, astrocytic and endothelial cell culture, and RNA-seq are provided in *SI Materials and Methods*.

ACKNOWLEDGMENTS. We thank R. Lifton for discussion and support, S. Artavanis-Tsakonas, R. Lifton, and E. Lo for critical comments, A. Lanahan for invaluable help with brain endothelial cell isolation, E. Grove, S. Ishibe, M. Lalioti, and B. Su for discussion, Y. Kawano and K. Ishigame for excellent technical assistance, C. Rahner and the Center for Cell and Molecular Imaging for assistance with electron microscopy, S. Mane and M. Mahajan for RNA sequencing, K. Bilguvar and K. Yasuno for help with bioinformatics, P. Theotokis for animal husbandry, and H. Chahboune for assistance with animal MRI. This work was supported by US National Institutes of Health Grants R01-NS046521 and R01-HL077357 and the Yale Program on Neurogenetics.

1. Russell DS, Rubenstein LJ (1989) *Pathology of Tumors of the Nervous System* (Williams and Wilkins, Baltimore).
2. Robinson JR, Awad IA, Little JR (1991) Natural history of the cavernous angioma. *J Neurosurg* 75:709–714.
3. Riant F, Bergametti F, Ayrignac X, Boulday G, Tournier-Lasserve E (2010) Recent insights into cerebral cavernous malformations: The molecular genetics of CCM. *FEBS J* 277:1070–1075.
4. Gault J, Shenkar R, Recksiek P, Awad IA (2005) Biallelic somatic and germ line CCM1 truncating mutations in a cerebral cavernous malformation lesion. *Stroke* 36:872–874.
5. Akers AL, Johnson E, Steinberg GK, Zabramski JM, Marchuk DA (2009) Biallelic somatic and germline mutations in cerebral cavernous malformations (CCMs): Evidence for a two-hit mechanism of CCM pathogenesis. *Hum Mol Genet* 18:919–930.
6. Pagenstecher A, Stahl S, Sure U, Felbor U (2009) A two-hit mechanism causes cerebral cavernous malformations: Complete inactivation of CCM1, CCM2 or CCM3 in affected endothelial cells. *Hum Mol Genet* 18:911–918.
7. Guzeloglu-Kayisli O, et al. (2004) KRIT1/cerebral cavernous malformation 1 protein localizes to vascular endothelium, astrocytes, and pyramidal cells of the adult human cerebral cortex. *Neurosurgery* 54:943–949.
8. Seker A, et al. (2006) CCM2 expression parallels that of CCM1. *Stroke* 37:518–523.
9. Tanriover G, et al. (2008) PDCD10, the gene mutated in cerebral cavernous malformation 3, is expressed in the neurovascular unit. *Neurosurgery* 62:930–938.
10. Plummer NW, et al. (2006) Neuronal expression of the Ccm2 gene in a new mouse model of cerebral cavernous malformations. *Mamm Genome* 17:119–128.
11. Whitehead KJ, Plummer NW, Adams JA, Marchuk DA, Li DY (2004) Ccm1 is required for arterial morphogenesis: Implications for the etiology of human cavernous malformations. *Development* 131:1437–1448.
12. Plummer NW, et al. (2004) Loss of p53 sensitizes mice with a mutation in Ccm1 (KRIT1) to development of cerebral vascular malformations. *Am J Pathol* 165:1509–1518.
13. McDonald DA, et al. (2011) A novel mouse model of cerebral cavernous malformations based on the two-hit mutation hypothesis recapitulates the human disease. *Hum Mol Genet* 20:211–222.
14. Whitehead KJ, et al. (2009) The cerebral cavernous malformation signaling pathway promotes vascular integrity via Rho GTPases. *Nat Med* 15:177–184.
15. Boulday G, et al. (2009) Tissue-specific conditional CCM2 knockout mice establish the essential role of endothelial CCM2 in angiogenesis: Implications for human cerebral cavernous malformations. *Dis Model Mech* 2:168–177.
16. Kleaveland B, et al. (2009) Regulation of cardiovascular development and integrity by the heart of glass-cerebral cavernous malformation protein pathway. *Nat Med* 15:169–176.
17. Harel L, et al. (2009) CCM2 mediates death signaling by the TrkA receptor tyrosine kinase. *Neuron* 63:585–591.
18. Hilder TL, et al. (2007) Proteomic identification of the cerebral cavernous malformation signaling complex. *J Proteome Res* 6:4343–4355.
19. Voss K, et al. (2007) CCM3 interacts with CCM2 indicating common pathogenesis for cerebral cavernous malformations. *Neurogenetics* 8:249–256.
20. Zawistowski JS, et al. (2005) CCM1 and CCM2 protein interactions in cell signaling: Implications for cerebral cavernous malformations pathogenesis. *Hum Mol Genet* 14:2521–2531.
21. Zhang J, Rigamonti D, Dietz HC, Clatterbuck RE (2007) Interaction between krit1 and malcavernin: Implications for the pathogenesis of cerebral cavernous malformations. *Neurosurgery* 60:353–359.
22. Li X, et al. (2010) Crystal structure of CCM3, a cerebral cavernous malformation protein critical for vascular integrity. *J Biol Chem* 285:24099–24107.
23. Goudreault M, et al. (2009) A PP2A phosphatase high density interaction network identifies a novel striatin-interacting phosphatase and kinase complex linked to the cerebral cavernous malformation 3 (CCM3) protein. *Mol Cell Proteomics* 8:157–171.
24. Fidalgo M, et al. (2010) CCM3/PDCD10 stabilizes GCKIII proteins to promote Golgi assembly and cell orientation. *J Cell Sci* 123:1274–1284.
25. Chen L, et al. (2009) Apoptotic functions of PDCD10/CCM3, the gene mutated in cerebral cavernous malformation 3. *Stroke* 40:1474–1481.
26. He Y, et al. (2010) Stabilization of VEGFR2 signaling by cerebral cavernous malformation 3 is critical for vascular development. *Sci Signal* 3:ra26.
27. Zheng X, et al. (2010) CCM3 signaling through sterile 20-like kinases plays an essential role during zebrafish cardiovascular development and cerebral cavernous malformations. *J Clin Invest* 120:2795–2804.
28. Tronche F, et al. (1999) Disruption of the glucocorticoid receptor gene in the nervous system results in reduced anxiety. *Nat Genet* 23:99–103.
29. Zhuo L, et al. (2001) hGFAP-cre transgenic mice for manipulation of glial and neuronal function in vivo. *Genesis* 31:85–94.
30. Gorski JA, et al. (2002) Cortical excitatory neurons and glia, but not GABAergic neurons, are produced in the Emx1-expressing lineage. *J Neurosci* 22:6309–6314.
31. Theis M, et al. (2003) Accelerated hippocampal spreading depression and enhanced locomotory activity in mice with astrocyte-directed inactivation of connexin43. *J Neurosci* 23:766–776.
32. Manning BD, Cantley LC (2007) AKT/PKB signaling: Navigating downstream. *Cell* 129:1261–1274.
33. Lo EH, Dalkara T, Moskowitz MA (2003) Mechanisms, challenges and opportunities in stroke. *Nat Rev Neurosci* 4:399–415.
34. Fruttiger M (2007) Development of the retinal vasculature. *Angiogenesis* 10:77–88.
35. Zerlin M, Goldman JE (1997) Interactions between glial progenitors and blood vessels during early postnatal corticogenesis: Blood vessel contact represents an early stage of astrocyte differentiation. *J Comp Neurol* 387:537–546.
36. Iadecola C, Nedergaard M (2007) Glial regulation of the cerebral microvasculature. *Nat Neurosci* 10:1369–1376.
37. Ward NL, Putoczki T, Mearow K, Ivanco TL, Dumont DJ (2005) Vascular-specific growth factor angiopoietin 1 is involved in the organization of neuronal processes. *J Comp Neurol* 482:244–256.
38. Fukuhara S, et al. (2008) Differential function of Tie2 at cell-cell contacts and cell-substratum contacts regulated by angiopoietin-1. *Nat Cell Biol* 10:513–526.
39. Thurston G, et al. (2005) Angiopoietin 1 causes vessel enlargement, without angiogenic sprouting, during a critical developmental period. *Development* 132:3317–3326.
40. Abe M, et al. (2005) Thrombus and encapsulated hematoma in cerebral cavernous malformations. *Acta Neuropathol* 109:503–509.
41. Trapnell C, et al. (2010) Transcript assembly and quantification by RNA-Seq reveals unannotated transcripts and isoform switching during cell differentiation. *Nat Biotechnol* 28:511–515.
42. Zhang J, Clatterbuck RE, Rigamonti D, Chang DD, Dietz HC (2001) Interaction between krit1 and icap1alpha infers perturbation of integrin beta1-mediated angiogenesis in the pathogenesis of cerebral cavernous malformation. *Hum Mol Genet* 10:2953–2960.
43. Zawistowski JS, Serebriiskii IG, Lee MF, Golemis EA, Marchuk DA (2002) KRIT1 association with the integrin-binding protein ICAP-1: A new direction in the elucidation of cerebral cavernous malformations (CCM1) pathogenesis. *Hum Mol Genet* 11:389–396.
44. Guo S, Lo EH (2009) Dysfunctional cell-cell signaling in the neurovascular unit as a paradigm for central nervous system disease. *Stroke* 40 (3 Suppl):S4–S7.
45. McCarty JH, et al. (2005) Selective ablation of alphav integrins in the central nervous system leads to cerebral hemorrhage, seizures, axonal degeneration and premature death. *Development* 132:165–176.
46. Ito S, Greiss S, Gartner A, Derry WB (2010) Cell-nonautonomous regulation of C. elegans germ cell death by kri-1. *Curr Biol* 20:333–338.
47. Ogilvy CS, Moayeri N, Golden JA (1993) Appearance of a cavernous hemangioma in the cerebral cortex after a biopsy of a deeper lesion. *Neurosurgery* 33:307–309.
48. Larson JJ, Ball WS, Bove KE, Crone KR, Tew JM, Jr. (1998) Formation of intracerebral cavernous malformations after radiation treatment for central nervous system neoplasia in children. *J Neurosurg* 88:51–56.
49. Denier C, et al. (2006) Genotype-phenotype correlations in cerebral cavernous malformations patients. *Ann Neurol* 60:550–556.
50. Gault J, Sain S, Hu LJ, Awad IA (2006) Spectrum of genotype and clinical manifestations in cerebral cavernous malformations. *Neurosurgery* 59:1278–1284.
51. Vikkula M, et al. (1996) Vascular dysmorphogenesis caused by an activating mutation in the receptor tyrosine kinase TIE2. *Cell* 87:1181–1190.